

KCFRC: Kinematic Collision-Aware Foothold Reachability Criteria for Legged Locomotion

Lei Ye, Haibo Gao, Huaiguang Yang, Peng Xu*, Haoyu Wang, Tie Liu, Junqi Shan, Zongquan Deng and Liang Ding*

Abstract—Legged robots face significant challenges in navigating complex environments, as they require precise real-time decisions for foothold selection and contact planning. While existing research has explored methods to select footholds based on terrain geometry or kinematics, a critical gap remains: few existing methods efficiently validate the existence of a non-collision swing trajectory. This paper addresses this gap by introducing KCFRC, a novel approach for efficient foothold reachability analysis. We first formally define the foothold reachability problem and establish a sufficient condition for foothold reachability. Based on this condition, we develop the KCFRC algorithm, which enables robots to validate foothold reachability in real time. Our experimental results demonstrate that KCFRC achieves remarkable time efficiency, completing foothold reachability checks for a single leg across 900 potential footholds in an average of 2 ms. Furthermore, we show that KCFRC can accelerate trajectory optimization and is particularly beneficial for contact planning in confined spaces, enhancing the adaptability and robustness of legged robots in challenging environments.

Index Terms—Legged robots, foothold planning, reachability analysis, collision avoidance, trajectory optimization, kinematic constraints.

I. INTRODUCTION

LEGGED robots have emerged as pivotal mobile platforms for executing complex tasks in unstructured environments. Navigating confined spaces necessitates meticulous motion planning and foothold selection to prevent limb collisions during leg swings. This poses a fundamental challenge: how to guarantee kinematically feasible, collision-free transitions between consecutively planned footholds, particularly when joint space limitations and dynamic body movements constrain the swing leg’s operational space. Formally, we define the **Foothold Reachability Problem (FRP)** as verifying the existence of a collision-free trajectory that connects two adjacent footholds under prescribed torso motion, considering both environmental obstacles and the robot’s kinematic constraints.

This work focuses on efficient **Foothold Reachability Criteria (FRC)** considering leg kinematic constraints and

The authors are with the State Key Laboratory of Robotics and Systems, Harbin Institute of Technology, Harbin 150001, China.

*Corresponding author: Peng Xu (pengxu_hit@163.com), Liang Ding (liangding@hit.edu.cn).

This work was supported by the National Key R&D Program of China (2022YFB4702300); the National Natural Science Foundation of China (Grant No. 91948202); the Fundamental Research Funds for the Central Universities (FRFCU9803500621, No. HIT-OCEF. 2023042); the Heilongjiang Postdoctoral Fund under Grant LBH-Z20136.

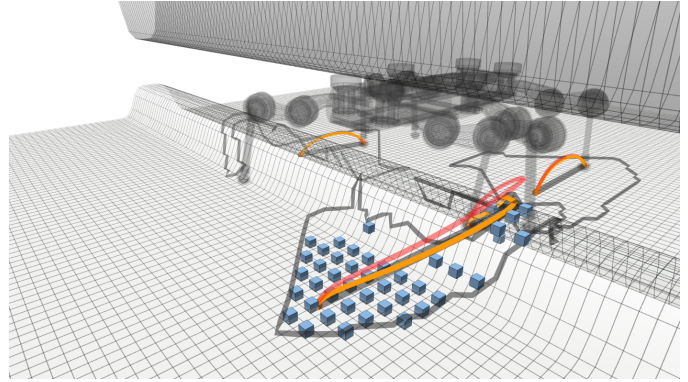


Figure 1: Kinematic Collision-Aware Foothold Reachability Criteria demonstration in barrier traversal. Blue cubes show validated reachable footholds, orange/red curves show initialized/optimized swing trajectories. The hexapod robot must carefully select footholds to navigate through the confined space. More supplemental materials are available at [KCFRC Webpage](#).

limb-terrain collision for legged locomotion, which plays a crucial role in legged robot contact planning. This is especially important for some non-mammalian configuration robots with joints exposed outside the base-ground projection [1] that easily collide with the environment.

As illustrated in Fig. 1, successful barrier traversal by the hexapod requires simultaneous satisfaction of multiple constraints: avoiding foot-ground collisions, preventing knee-ceiling interference, and maintaining kinematic feasibility throughout the motion.

While the FRP shares similarities with classical motion planning problems, existing approaches have limitations for real-time legged locomotion applications. Classical sampling-based planners such as PRM and RRT* can provide probabilistically complete solutions for reachability queries, but typically require substantial computation time (tens to hundreds of milliseconds) that exceeds real-time planning requirements. Recent advances in convex-set methods for manipulator motion planning, particularly Graph of Convex Sets (GCS) [2], offer elegant solutions but require complex geometric reasoning [3] and struggle with the dynamic nature of moving-base scenarios in legged locomotion. GPU-accelerated batch inverse kinematics approaches, such as cuRobo [4] and similar frameworks, can achieve fast collision checking during trajectory sampling but require specialized hardware, significant memory overhead

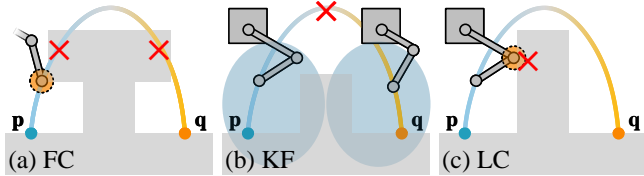


Figure 2: Foothold Evaluation Criteria. (a) Foot Collision checking for foot-terrain interference, (b) Kinematic Feasibility ensuring joint limits compliance, and (c) Leg Collision detecting segment-obstacle interference. These criteria require explicit trajectory generation for validation.

for collision representation maintenance, and typically operate as post-hoc filters rather than providing a priori reachability guarantees.

For legged robot specific approaches, Fahmi et al. proposed Foothold Evaluation Criteria (FEC) for reachability checks on predefined swing trajectories [5], as shown in Fig. 2. This method considers foot collision, kinematic feasibility, and leg collision while being limited to fixed trajectory patterns. Implicit contact planning methods such as MPC/WBC-based controllers [6], [7] and RL controllers [8] formulate the planning-control problem with related constraints and heuristic reference trajectories but do not provide explicit reachability guarantees before trajectory optimization. Without efficient reachability pre-screening, these methods may struggle with corner cases like Fig. 1 or waste computational resources on infeasible problems.

This paper proposes **Kinematic Collision-Aware Foothold Reachability Criteria** for legged robot contact planning, called **KCFRC**. Our method provides a computationally efficient approach to foothold reachability analysis that complements existing trajectory planning methods. It offers a unique combination of theoretical guarantees and computational efficiency specifically designed for real-time legged locomotion applications. We define the FRP for legged robots mathematically and demonstrate a sufficient condition for swing trajectory existence using topological analysis. The method is implemented and validated on the EISpider 4 Air robot.

To the best of our knowledge, our approach is the first to provide theoretical guarantees about foothold reachability while serving as a fast preprocessing filter that can reduce computational burden for subsequent trajectory planning. The method achieves significant speed improvements (100-400x faster than sampling-based methods) while maintaining high accuracy for the specific case of 3-DOF leg chains. The key contributions of this work include:

- 1) **A theoretical framework providing sufficient conditions for foothold reachability.** We formulate the FRP mathematically and demonstrate a topologically-based sufficient condition that enables rapid reachability assessment without full trajectory optimization.
- 2) **An efficient algorithmic implementation with substantial computational improvements.** We combine the proposed theoretical sufficient conditions with practical

collision and kinematic constraint checking to develop a fast foothold reachability assessment method. The open-source implementation¹ achieves 100-400x speed improvements over existing methods while maintaining high accuracy.

- 3) **Comprehensive validation across multiple robot platforms and environments.** The method is validated through extensive simulation and hardware experiments on the EISpider 4 Air hexapod and Unitree A1 quadruped robots, demonstrating its generalizability across different morphologies and its effectiveness in real-world confined space navigation scenarios.

II. RELATED WORK

A. Reachability in Robotics

Reachability in robotics varies across applications. In navigation, traversability maps [9], [10] define robot-accessible regions using terrain and motion constraints. For manipulators, reachability maps characterize end-effector pose accessibility [11], with recent advances using convex set graphs for planning efficiency [2] and dynamic grasping [12].

In legged locomotion, sequential reachability constraints for torso poses [13]–[15] often neglect detailed foothold analysis. Implicit planning methods like MPC [7] and RL [8] risk failure in confined spaces by overlooking foothold/trajectory reachability, highlighting the need for integrated reachability validation.

B. Foothold Reachability from Terrain Perspective

Early foothold selection methods focused primarily on terrain morphology. Kolter et al. [16] introduced terrain-aware control using foot-cost maps derived from height map features, while Kalakrishnan et al. [17] improved this through expert demonstration-based foothold ranking. Similar terrain-based approaches analyzing inclination, roughness, and geometry have been validated across various platforms [18]–[20].

C. Foothold Reachability from Kinematics Perspective

Nevertheless, footholds should not be determined solely by terrain without considering robot kinematics. Fankhauser et al. [6] and Jenelten et al. [21] developed ANYmal locomotion planners incorporating foothold-score maps with kinematic feasibility constraints, while Grandia et al. [7] used polygon dilation to reduce computational demand. Although these methods reflect foothold reachability through optimization constraints, they do not explicitly define reachability or ensure the existence of non-collision swing trajectories.

Foothold Evaluation Criteria (FEC) [5] assess foot collision, kinematic feasibility, and leg collision along predefined swing trajectories (Fig. 2). CNN acceleration methods [22] further optimize FEC computation. However, this approach fails to rigorously assess the existence of feasible swing trajectories, relying instead on validity checks confined to predefined candidate trajectories or simplistic heuristics such as maximum step height thresholds.

¹<https://github.com/MasterYip/FLTPlanner>

D. Foothold Reachability Check through Trajectory Planner

Trajectory planners have been applied for swing trajectory planning in works [6], [23] after footholds are decided. Intuitively, they can solve foothold reachability by searching for feasible swing trajectories between adjacent footholds given torso trajectory. However, checking foothold reachability in batches using trajectory planners is inefficient. Although sampling-based planners like PRM [24] and RRT [25] are probabilistically complete, they typically require exhaustive sampling and substantial computation time in solving FRP that exceeds real-time requirements. Gradient-based planners [26], [27] suffer from local minima and require initial trajectories. Recent convex-set methods like Graph of Convex Sets (GCS) [2] offer elegant solutions but require complex geometric reasoning [3] and struggle with moving-base scenarios in legged locomotion. GPU-accelerated approaches like cuRobo [4] achieve fast collision checking but require specialized hardware and operate as post-hoc filters rather than providing a priori reachability guarantees.

III. OVERVIEW OF THE WORK

The paper's structure follows the framework illustrated in Fig. 4. We first formulate the FRP in Section IV-A, followed by deriving a sufficient foothold reachability condition in Section IV-B. Section V details the KCFRC implementation through four sequential stages (Fig. 4b-e), supplemented by an explanatory animation². Section VI analyzes its performance through quantitative benchmarks, while Section VII demonstrates applications KCFRC. The work concludes in Section VIII.

IV. FOOTHOLD REACHABILITY PROBLEM

A. Problem Formulation and Simplification Assumption

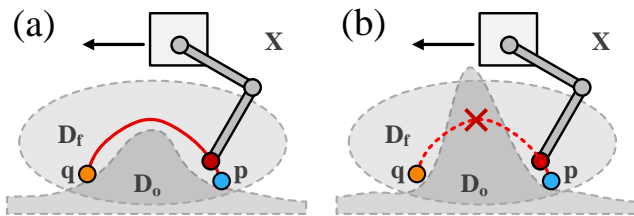


Figure 3: Reachability of the expected foothold. The foothold is reachable if feasible domain is not split by obstacles, and vice versa.

Definition 1 (Foothold Reachability). *As is shown in Fig. 3, we define the reachability of a foothold as below. Given torso trajectory and robot specifications, the next foothold is reachable only if the following conditions are met:*

- 1) *Trajectory Existence (TE): There exists a swing trajectory connecting lift-off and touch-down footholds during base movement.*

²https://masteryip.github.io/fltplanner.github.io/static/videos/method_standalone.mp4

Table I
SYMBOL & ABBREVIATION

Symbols	Description
p	Current foothold
q	Candidate foothold
X	Space used in the FRP
D_f	Feasible domain in the FRP
D_o	Occupied domain in the FRP
$f_P : \mathbb{E}^3 \rightarrow \text{SE}(3)$	Torso pose query function
$f_G : \mathbb{E}^2 \rightarrow \mathbb{R}$	Ground elevation function
$f_C : \mathbb{E}^2 \rightarrow \mathbb{R}$	Ceiling elevation function
S_g	Guiding surface
$f_{S_g} : \mathbb{E}^2 \rightarrow \mathbb{R}$	Guiding surface elevation function
S_a	Auxiliary surface
$f_{S_a} : \mathbb{E}^2 \rightarrow \mathbb{R}$	Auxiliary surface elevation function
B	2D Intersection Border of $S_a \cap D_f$
i	Leg index
Abbreviations	Description
KCFRC	Kinematic Collision-Aware Foothold Reachability Criteria
FRP	Foothold Reachability Problem
FEC	Foothold Evaluation Criteria
TE	Trajectory Existence
KF	Kinematic Feasibility
NFC	No Foot Collision
NLC	No Leg Collision

- 2) *Kinematic Feasibility (KF): Joint limits are satisfied at each point of the trajectory.*
- 3) *No Foot Collision (NFC): The foot does not collide with the terrain during the swing phase.*
- 4) *No Leg Collision (NLC): Any part of the leg does not collide with the terrain during the swing phase.*

To clarify this problem, we formulate the reachability problem mathematically as follows.

Problem 1 (Reachability Problem). *Let $D_f, D_o \subseteq X$ be non-empty subsets of a topological space X , where D_f is a connected closed set and D_o is an open set. Given points p, q such that $p, q \in D_f$, $p, q \notin D_o$, and $p \neq q$. Determine an efficient method to decide whether there exists a path $f : [0, 1] \rightarrow (D_f \setminus D_o)$ such that $p = f(0)$ and $q = f(1)$.*

This problem is the mathematical abstraction of FRP, the following assumptions are proposed to make this problem concrete.

Assumption 1 (Assumption for FRP). *For the consideration of computational feasibility, this project has the following specific requirements for the problem:*

- (1) *X is the three-dimensional Euclidean space \mathbb{E}^3 .*
- (2) *D_f is a three-dimensional connected feasible domain. We assume the robot torso trajectory is known during a single step, and there exists a continuous map $f_P : \mathbb{E}^3 \rightarrow \text{SE}(3)$ such that for every point s in D_f exists a corresponding robot base pose $f_P(s)$ satisfies Kinematic Feasibility (KF) and No Leg Collision (NLC) conditions. The specific definition of D_f and leg collision checking method will be introduced later.*
- (3) *D_o is the occupied domain of the three-dimensional terrain, including ceiling and ground. It can be represented*

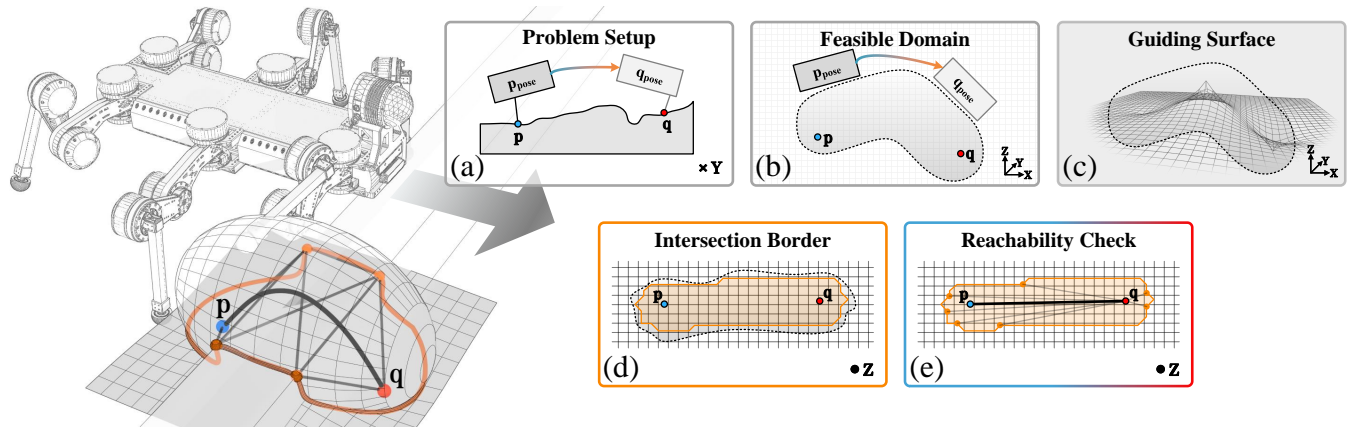


Figure 4: Overview of KCFRC. (a) Problem setup. (b) Feasible domain definition [Section V-C]. (c) Guiding surface generation [Section V-D]. (d) Intersection border computing [Section V-E]. (e) Reachability check [Section V-F].

as

$$D_o : \{(x, y, z) \in X \mid z < f_G(x, y), z > f_C(x, y)\}$$

where $f_G(x, y)$ is the height map of the terrain, and $f_C(x, y)$ is the height map of the ceiling. Both are single-valued continuous functions, and $f_G(x, y) < f_C(x, y), \forall (x, y) \in \mathbb{E}^2$.

(4) p, q are the adjacent footholds of a leg in one step. They satisfy $p, q \in \{(x, y, z) \in X \mid z = f_G(x, y)\}$.

Remark 1. Under this assumption, D_f is a time-invariant feasible domain. However, the robot is moving during locomotion, hence some approximations are adopted when defining D_f .

B. Sufficient Condition for Foothold Reachability

Lemma 1. For Problem 1, if $D_f \setminus D_o$ is homeomorphic to D_f , then there exists a path $f : [0, 1] \rightarrow (D_f \setminus D_o)$ such that $p = f(0)$ and $q = f(1)$.

Intuitively, Lemma 1 is a sufficient condition for foothold reachability. Nevertheless, it is not practical for algorithm implementation. Therefore, we introduce the concept of guiding surface, which acts as a reference and helps in dimension reduction.

Definition 2 (Guiding Surface S_g). For problem 1, under the conditions of Assumption 1, if a single-connected two-dimensional surface S_g satisfies the following conditions:

(1) $S_g : \{(x, y, z) \in X \mid z = f_{S_g}(x, y)\}$, where f_{S_g} is a single-valued continuous function.

(2) $p, q \in S_g$.

then S_g is called a guiding surface.

Lemma 2 (Existence of Guiding Surface). For problem 1, under the conditions of Assumption 1, a guiding surface S_g must exist.

Proof. Since $p, q \in \{(x, y, z) \in X \mid z = f_G(x, y)\}$ and $f_G(x, y)$ is a single-valued continuous function, we can take $S_g : \{(x, y, z) \in X \mid z = f_G(x, y)\}$ as the guiding surface. Proof completed. \square

Remark 2. Although the existence of the guiding surface S_g is evident, the significance of the guiding surface lies in

providing a default reachable trajectory without considering terrain influences. Therefore, designing the guiding surface S_g should ideally satisfy that $S_g \cap D_f$ is single-connected. However, a guiding surface that meets this condition may not always exist.

After that, we define the auxiliary surface S_a to ensure that S_a does not intersect with the ceiling and ground.

Definition 3 (Auxiliary Surface S_a). For problem 1, under the conditions of Assumption 1, if there exists a guiding surface S_g , then an auxiliary surface $S_a : \{(x, y, z) \in X \mid z = f_{S_a}(x, y)\}$ can be defined as follows:

$$f_{S_a}(x, y) = \begin{cases} f_G(x, y), & \text{if } f_G(x, y) > f_{S_g}(x, y) \\ f_C(x, y), & \text{if } f_C(x, y) < f_{S_g}(x, y) \\ f_{S_g}(x, y), & \text{otherwise} \end{cases} \quad (1)$$

Theorem 1 (Sufficient Condition for Reachability). For problem 1, under the conditions of Assumption 1, if the auxiliary surface S_a corresponding to the guiding surface S_g satisfies that $S_a \cap D_f$ is connected, then there exists a path $f : [0, 1] \rightarrow (D_f - D_o)$, satisfying $p = f(0), q = f(1)$.

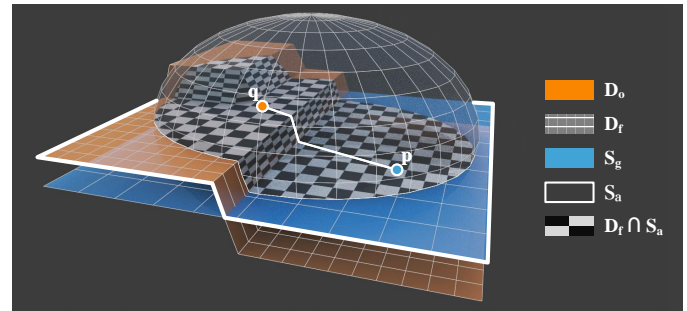


Figure 5: Diagram of the Sufficient Condition for Reachability (Theorem 1).

Proof. Since $D_o : \{(x, y, z) \in X \mid z < f_G(x, y), z > f_C(x, y)\}$, we have $S_a \cap D_o = \emptyset$, so $S_a \cap (D_f - D_o) = S_a \cap D_f$. Given that $S_a \cap D_f$ is connected, it follows that $S_a \cap (D_f - D_o)$

is connected, hence there exists a path $f : [0, 1] \rightarrow (D_f - D_o)$, satisfying $p = f(0), q = f(1)$. \square

As long as D_f, D_o, S_g, p, q are decided, it is possible to check the foothold reachability according to Theorem 1. The establishment of D_f, D_o, S_g will be discussed in the following sections. It is worth noting that the condition in Theorem 1 is a sufficient condition for the existence of solutions to the non-collision swing trajectory. However, a well-defined guiding surface may adapt to most cases in legged robot locomotion.

V. KINEMATIC COLLISION-AWARE FRC

A. Terrain Representation

We represent the environment and obstacles in the form of Grid Map [28], which is widely used in legged locomotion. To represent obstacles in confined spaces, the ground and ceiling layers are both defined and generated in real-time.

B. Kinematics and Collision Detection

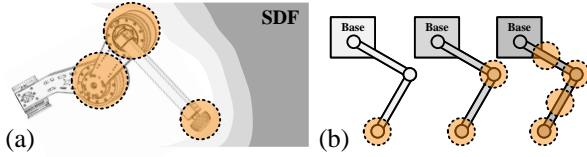


Figure 6: Collision detection method. (a) Collision detection under SDF. (b) Foot-collision-only, joint-collision-only and link-subdivision collision models.

Leg kinematics and inverse kinematics are computed using Pinocchio [29] and IKFast [30], respectively. For collision detection, we compute the Signed Distance Field (SDF) from the grid map asynchronously in a separate thread and model collision volumes using sets of spheres (Fig. 6). This sphere-based approach enables efficient collision validation through distance queries against the precomputed SDF.

C. Feasible Domain

For a 3-DOF robot leg, the conversion from configuration space C to task space T is a surjective mapping that may become bijective with appropriate joint limits. The space-time feasible domain D_{fi} represents the region swept by task space T_i during single-step movement:

$$D_{fi} : \{(x, y, z, t) \mid (x, y, z) \in T_i(t), t_0 < t < t_1\} \quad (2)$$

Since D_f is defined in the space-time domain which causes troubles in calculation, we introduce the **Pose Interpolation Task Domain (PITD)** approximation. Given base poses $P_p, P_q \in \text{SE}(3)$ and leg task space T_{ib} under base coordinates, we compute interpolated task spaces as shown in Fig. 7.

The PITD formulation addresses foothold reachability by approximating the continuous leg workspace evolution during robot base movement. As the robot transitions from pose P_p to P_q , the interpolation parameter $r(s) = l_{ps_{\perp}}/l_{pq} \in [0, 1]$ represents the progression along this transition:

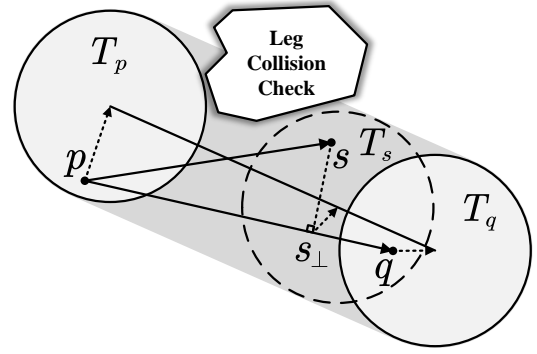


Figure 7: Approximate feasible domain PITD.

$$f_P^{PITD}(r) = \exp(r \cdot \log(P_q P_p^{-1})) \cdot P_p$$

$$T_s(r) = f_P^{PITD}(r) \cdot T_{ib}$$

Here, $f_P^{PITD}(r)$ computes the interpolated robot base pose using SE(3) exponential mapping, while $T_s(r)$ gives the leg's reachable workspace at the interpolated pose. This enables efficient evaluation of whether candidate footholds remain kinematically accessible throughout the robot's base motion.

The PITD feasible domain for leg i is then defined as:

$$D_f^{PITD} = \{s \mid s \in T_s(r(s)), \text{LegColl}(s) \neq \text{True}\} \quad (3)$$

where IKFast verifies kinematic feasibility and precomputed gridmap SDF ensures collision-free conditions according to Section V-B.

D. Guiding Surface Design

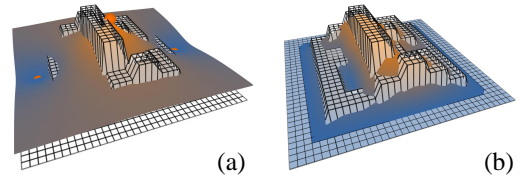


Figure 8: Grid map and generated guiding surfaces. (a) Keypoint-weighted guiding surface creates smooth interpolation between key points with $k = 1, w_i = 1$. (b) Convolutional guiding surface smooths terrain features using $n = 5, l = 0.03$ m kernel. The grid map resolution is 0.05 m.

The guiding surface S_g plays a crucial role in creating the auxiliary surface S_a that helps determine foothold reachability. Intuitively, S_g acts as a "bridge" that guides the leg motion between start and goal positions, ensuring that the intersection $S_a \cap D_f$ forms a connected domain for efficient reachability analysis. The surface should smoothly connect the start and goal footholds while avoiding major obstacles, creating a feasible pathway for leg swing motion.

Keypoint-Weighted Guiding Surface. This approach creates a smooth surface by interpolating between strategically placed keypoints. The guiding surface $S_g : \{(x, y, z) \in$

$X \mid z = f_{S_g}(x, y)$ is constructed using keypoints $B = \{p_1, p_2, \dots, p_n\}$ through inverse distance weighting:

$$f_{S_g}(x, y) = \frac{\sum_{i=1}^n \frac{w_i z_i}{r_i^k}}{\sum_{i=1}^n \frac{w_i}{r_i^k}} \quad (4)$$

where $p_i = (x_i, y_i, z_i)$ are the keypoints, $r_i = \|(x, y) - (x_i, y_i)\|$ is the Euclidean distance from point (x, y) to keypoint i , w_i is the influence weight of keypoint p_i , and k controls the smoothness (higher k creates sharper transitions). For FRP, we set p_1 and p_n as the start and goal positions, with intermediate keypoints sampled along the connecting line to create a natural pathway. As visualized in Fig. 8(a), this creates a smooth surface that naturally guides the leg motion around obstacles.

Convolutional Guiding Surface. For batch foothold reachability checks where specific goal positions are not predetermined, we employ a terrain-adaptive approach. The guiding surface smooths local terrain variations through convolution with the ground elevation map:

$$f_{S_g}(x, y) = \frac{\sum_{i,j=1}^n f_G(x + (i - \frac{n+1}{2})l, y + (j - \frac{n+1}{2})l)}{n^2} \quad (5)$$

where n is the convolution kernel size (odd number), l is the grid spacing, and f_G is the ground elevation function. This averaging operation removes sharp terrain features that could fragment the feasible domain, creating a smoother surface for more robust reachability analysis as shown in Fig. 8(b).

E. Intersection Border Search

After S_g and S_a are obtained, it becomes possible to search the intersection border, representing $S_a \cap D_f$ in the 2D form that comes with better performance. As is shown in Fig. 9, we search the intersection border directly on the grid map for simplicity.

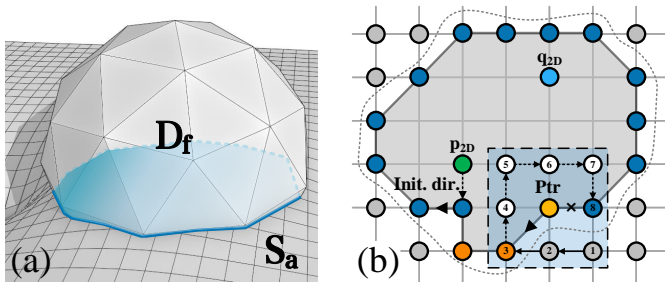


Figure 9: 2D intersection border search. (a) Intersection of D_f and S_a . (b) schematic diagram of Algorithm 1.

Algorithm 1 computes intersection border B given the feasible domain D_f , auxiliary surface f_{S_a} , start point p and goal point q .

F. Reachability Check

Visibility graph is introduced for reachability judgment. As is shown in Fig. 10, it can be proved that the shortest path from start to goal consists of line segments among start p , goal q and concave points of the projected 2D connected domain,

Algorithm 1 2D Intersection Border Search

Input: D_f, f_{S_a}, p, q

Output: B

```

1: Find nearest grid index  $p_{2D}, q_{2D}$  of  $p, q$ .
2:  $Ptr \leftarrow$  First border point index.
3:  $B.append(Ptr)$ 
4: while  $Ptr \neq B[0]$  or  $len(B) < 3$  do
5:   for  $\delta \in$  index around  $Ptr$  clockwise do
6:     if  $3DPos(\delta, f_{S_a})$  is in  $D_f$  for the first time then
7:        $Ptr \leftarrow \delta$ 
8:        $B.append(Ptr)$ 
9:     break
10:  end if
11: end for
12: end while
13: return  $B$ 
    
```

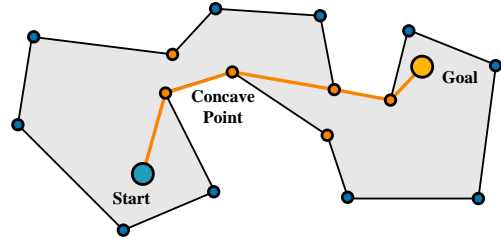


Figure 10: Shortest path in projected 2D feasible domain. The shortest path in this domain goes through concave points and connects start and goal points.

besides, adjacent points on the shortest path must be visible to each other. If the goal in the projected 2D connected domain is reachable, then the shortest path connecting p and q exists. Therefore, the goal is **reachable** if and only if the goal q is visible to start point p or any concave point on the intersection border B . Algorithm 2 describes the major steps of KCFRC.

Algorithm 2 Kinematic Collision-Aware FRC

Input: $p, q, P_p, P_q, i, f_G, f_C$

Output: bool

```

1: Calculate SDF of  $f_G$  and  $f_C$  ▷ Section V-B
2: Generate  $S_g$  ▷ Eq. (4) or (5)
3: Obtain  $f_{S_a}$  from  $f_{S_g}, f_G, f_C$  ▷ Eq. (1)
4: Construct  $D_f^{PITD}$  ▷ Eq. (3)
5:  $B \leftarrow$  IntersectBorder( $D_f^{PITD}, f_{S_a}, p, q$ ) ▷ Alg. 1
6: Obtain concave points  $P_{concave}$  from  $B$ 
7: Set up  $VisGraph(p_{2D}, q_{2D}, P_{concave})$  ▷ Section V-F
8: for  $x \in \{p_{2D}\} \cup P_{concave}$  do
9:   if Visible( $x, q_{2D}$ ) then
10:    return True
11:   end if
12: end for
13: return False
    
```

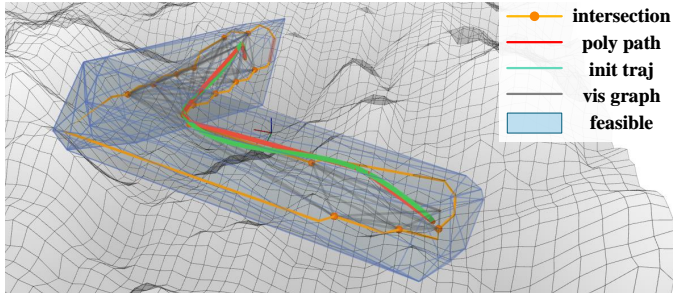


Figure 11: Reachability check experiment. Random convex polyhedra corridor is generated as the feasible domain, and stochastic fractal grid map as obstacles. Meanwhile, the shortest polygon path, visibility graph, and initialized trajectory are visualized.

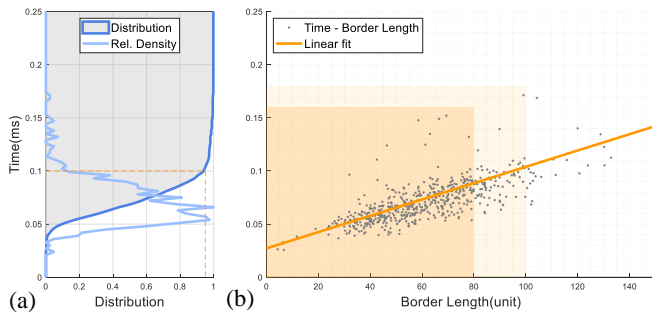


Figure 12: Reachability check time w.r.t intersection border length. Linear fitting of the data is $y = ax + b$, $a = 0.00077$, $b = 0.02722$.

VI. EXPERIMENT RESULTS

To illustrate the performance of KCFRC, we conduct an experiment that examines its time performance and scalability, and compare it to other methods. All experiments were conducted on an Intel NUC12WSKi7 (Intel® Core™ i7-1260P) running Ubuntu 20.04 LTS and ROS Noetic. The algorithms were executed entirely on the CPU without any GPU acceleration.

A. Time Performance and Scalability

Our algorithm is tested in generated scenarios to assess KCFRC performance. Fig. 11 shows one experiment scenario with a 60×60 fractal noise grid map and randomly generated feasible domain using 3D QuickHull [31]. Start and goal points are randomly selected at corridor ends for reachability checking, with kinematic and leg collision checks replaced by convex hull checks.

We evaluate computational performance across 1,000 test cases, recording intersection border length and processing time. Fig. 12(a) shows 95% of cases resolve within 0.1 ms (0.04-0.1 ms typical range). Fig. 12(b) demonstrates linear scaling with border size, with computation consistently under 0.16 ms for border lengths below 80 units and maximum time below 0.2 ms, meeting real-time requirements.

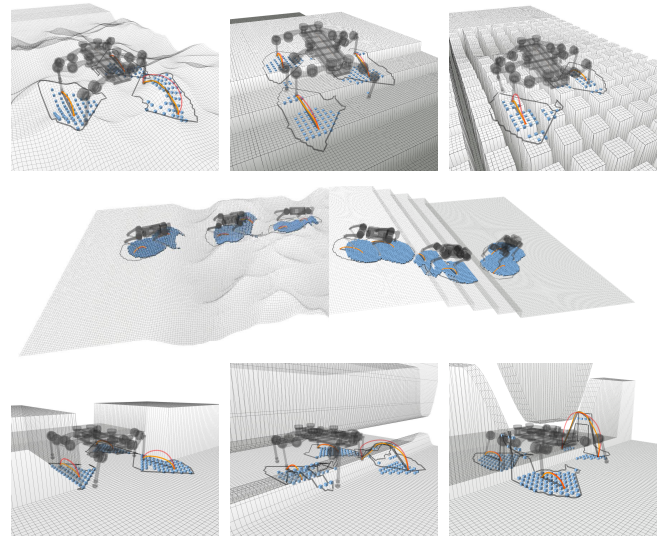


Figure 13: Representative planning scenes for foothold reachability check comparison. **Top Left&Mid:** Hexapod dense planning scenes. **Top Right:** Hexapod sparse planning scenes. **Mid-Row:** Quadraped dense planning scenes. **Bottom Row:** Hexapod confined planning scenes. Planned contact states are recorded for foothold reachability check benchmarking. The grid map resolution is set to 2.5 cm/grid.

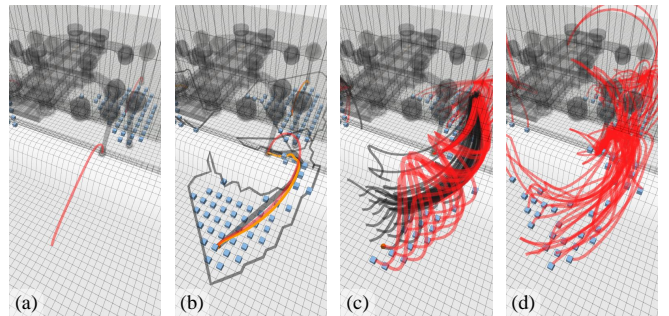


Figure 14: Foothold reachability check methods participate in the reachability check experiment for comparison. (a) FEC with predefined swing trajectory. (b) KCFRC. (c) RRT-Connect. (d) STOMP.

B. Foothold Reachability Check Comparison

1) *Planning Scenes Setup:* To systematically evaluate KCFRC's performance in foothold reachability check, we benchmark different methods on EISpider 4 Air hexapod and Unitree A1 quadraped in several representative planning scenes (Fig. 13). For each scene, contact states are precomputed by the MCTS planning pipeline [14] and stored. During execution, these states are reloaded to perform foothold reachability checks. For every swing leg transition between consecutive contact states, we sample **900 candidate footholds** (arranged in a 30×30 structured grid with 0.025 m resolution) around the nominal foothold position of the target state, ensuring total coverage of legs' task space.

2) *Methods for Comparison*: As shown in Fig. 14, the methods participating in this experiment are as follows, with their key parameters listed in Table II:

- **KCFRC (keypoint-weighted guiding surface)**. Provides higher accuracy by updating the intersection border for every candidate foothold. It is suitable for cluttered or confined environments where accuracy is critical.
- **KCFRC (convolutional guiding surface)**. Optimized for speed by updating the intersection border once per leg. It is ideal for sparse or real-time applications where computational efficiency is paramount.
- **RRT-Connect** [32]. We implement a collision validator and enforce monotonic time-increasing constraints in the configuration space. If a valid path is generated within the time limit, the target foothold is considered reachable.
- **STOMP** [33]. We set up STOMP to optimize the trajectory initialized from a linear interpolated one in configuration space, applying the constraints mentioned in previous sections as soft constraints. If the algorithm ends up with a valid trajectory, the candidate foothold is deemed reachable.
- **FEC** [5]. We examine the predefined swing trajectory according to FEC. The swing trajectory clears the maximum sampled grid map height on the line connecting adjacent footholds. If no violation of FEC is detected, it is regarded as a reachable foothold.

Table II
KEY PARAMETERS OF THE METHODS

Parameters	Value	Description
Robot		
ElAir Knee	0.05 m	Knee collision ball radius.
ElAir Foot	0.03 m	Foot collision ball radius.
A1 Knee	0.03 m	Knee collision ball radius.
A1 Foot	0.02 m	Foot collision ball radius.
Ground Truth		
Traj Space	-	Configuration space.
Max Step	0.6	Max search step in configuration space.
Max Time	10s	Max search time.
Max Retry	5	Retry till success up to 5 times.
RRT-Connect		
Traj Space	-	Configuration space.
Max Step	0.4	Max search step in configuration space.
Max Time	1ms/50us	Max search time.
STOMP		
Traj Space	-	Configuration space.
Resolution	20	Trajectory resolution in optimization.
Max Iters	100	Max iterations.
Rollout Num	10	Number of rollouts for sampling.
FEC		
Traj Space	-	Euclidean space.
Traj Gen	-	2-Stage Hermite (apex clears max height).
Resolution	50	Resolution of criteria evaluation.

While all the methods nominally address kinematic feasibility, foot collision, and leg collision constraints, no existing approach provides rigorous reachability verification. To compare these methods' accuracy, precision and recall rates, we establish an **Exhaustive RRT baseline** as the **Ground Truth** method (see Table II). This exhaustive RRT provides a probabilistically complete reference by allowing extensive

search time (up to 10s per foothold with max 5 retries) to thoroughly explore the configuration space. The method ensures reliable ground truth establishment by eliminating concerns about circular validation, as it operates independently from our proposed KCFRC approach using fundamentally different search principles.

Table III
FOOTHOLD REACHABILITY CHECK COMPARISON

Method	Ave. Time(ms)	Max. Time(ms)	Ave. Accuracy	Ave. Precision	Ave. Recall
Hexapod Confined Planning Scenes					
Ground Truth	827.852	18941.200	1.000	1.000	1.000
KCFRC(key)	50.574	78.740	0.996	0.998	0.986
KCFRC(conv)	2.580	4.070	0.993	0.999	0.974
RRT-C(1ms)	303.257	1085.290	0.998	1.000	0.992
RRT-C(50us)	209.600	948.055	0.972	1.000	0.889
STOMP	796.161	5099.620	0.976	0.999	0.908
FEC	10.226	36.722	0.948	1.000	0.796
Hexapod Dense Planning Scenes					
Ground Truth	458.751	5193.540	1.000	1.000	1.000
KCFRC(key)	47.467	83.766	0.996	1.000	0.987
KCFRC(conv)	2.384	5.295	0.994	1.000	0.977
RRT-C(1ms)	181.670	460.035	0.998	1.000	0.990
RRT-C(50us)	90.465	333.077	0.972	1.000	0.892
STOMP	309.474	1891.580	0.992	1.000	0.968
FEC	9.494	35.968	0.943	1.000	0.782
Quadruped Dense Planning Scenes					
Ground Truth	654.656	7022.720	1.000	1.000	1.000
KCFRC(key)	33.559	58.345	0.994	1.000	0.982
KCFRC(conv)	1.909	4.536	0.978	1.000	0.934
RRT-C(1ms)	587.400	2004.230	0.996	1.000	0.989
RRT-C(50us)	470.874	1706.380	0.962	1.000	0.889
STOMP	966.210	4507.900	0.985	1.000	0.955
FEC	5.306	12.778	0.920	1.000	0.765
Hexapod Sparse Planning Scenes					
Ground Truth	103.470	352.172	1.000	1.000	1.000
KCFRC(key)	27.376	68.729	0.998	1.000	0.984
KCFRC(conv)	1.627	2.748	0.997	1.000	0.978
RRT-C(1ms)	90.888	350.998	0.999	1.000	0.992
RRT-C(50us)	46.812	167.921	0.984	1.000	0.898
STOMP	74.021	543.723	0.999	1.000	0.994
FEC	6.070	14.660	0.984	1.000	0.900

3) *Performance Metrics*: Through all the planning scenes and planned contact states mentioned above, computation time and binary reachability matrices (30×30) are collected for each leg in a single contact state transition. Table III shows the time performance (per leg, 900 candidate footholds) and the accuracy, precision, and recall rates (of all footholds) of these methods in confined, dense, and sparse scenes respectively.

4) *Method Comparison*: The experimental results demonstrate KCFRC's effectiveness across different scene types and robot morphologies. KCFRC(key) consistently achieves high accuracy levels (99.4-99.8%) comparable to RRT-Connect(1ms) (99.6-99.9%) while maintaining excellent recall rates (98.2-98.7% vs. 98.9-99.2%), validating KCFRC's theoretical foundation as both methods can identify nearly all reachable footholds with similar reliability. However, the computational efficiency advantage is substantial: KCFRC(key) operates 6-18 \times faster than RRT-Connect(1ms) across all scenarios (27.4-50.6ms vs. 90.9-587.4ms), while KCFRC(conv) achieves remarkable speed improvements of 100-400 \times (1.6-2.6ms) with only modest accuracy degradation (97.8-99.7%

accuracy, 93.4-97.8% recall). In contrast, FEC demonstrates consistent limitations across challenging terrains, achieving only 76.5-90.0% recall despite perfect precision, confirming its inadequacy for complex environments where predefined trajectories frequently fail.

Morphology adaptability is confirmed through quadruped validation, where KCFRC maintains high performance (99.4% accuracy, 98.2% recall for key variant) while benefiting from reduced kinematic complexity (33.6ms vs. 47.5ms for hexapod dense scenes). These results establish KCFRC(key) as the optimal choice for accuracy-critical applications requiring reliability comparable to exhaustive planners, while KCFRC(conv) serves real-time applications where computational efficiency is paramount, delivering 100-400 \times speedup over traditional methods while maintaining >97% accuracy.

FEC's poor performance in confined spaces stems from its reliance on predefined swing trajectories that follow simplistic apex-clearing rules. In complex environments (barriers, tunnels), these rigid trajectories frequently collide with obstacles even when alternative feasible paths exist, explaining the 15-20% recall degradation compared to KCFRC's adaptive path planning approach.

5) *Advantages & Limitations:* KCFRC demonstrates several significant advantages over existing methods:

- **Time Efficiency.** It outperforms all other methods in the time efficiency index, achieving microsecond-scale computation.
- **High Accuracy.** KCFRC(conv) shows only marginal degradation from KCFRC(key) while maintaining >97% accuracy.
- **Complex Environment Adaptation.** Although confined environments seriously affect FEC accuracy, KCFRC maintains the same level as planner-based methods through its ability to identify multiple feasible pathways rather than being constrained to predefined trajectories.

As a sufficient condition approach, KCFRC may occasionally classify reachable footholds as unreachable (false negatives) in specific scenarios:

- **Narrow Configuration Tunnels:** When feasible paths involve very narrow passages that guiding surface smoothing cannot adequately represent.
- **Multi-Modal Solutions:** In scenarios with multiple disconnected feasible regions, alternative pathways requiring significant configuration space detours may be missed.
- **Guiding Surface Constraints:** Generation failures for subtle terrain features in highly irregular or fractal-like obstacle configurations.
- **Resolution Dependencies:** Conservative margin settings may classify trajectories as infeasible at discretized domain boundaries where narrow gaps theoretically allow passage.

These limitations result in false negative rates of 1-6% depending on scene complexity, robot platform and variant choice while maintaining zero false positives for safety-critical applications.

Table IV
COMPARISON OF SWING TRAJECTORY PLANNING
PERFORMANCE

Planners in Config Space		Time (ms)	Len. (rad)	Cost (s^{-3})	Succ. Num.	Succ. Rate
Proposed	Mean	0.818	2.440	140.117	493	0.992
	Max.	12.509	8.031	6079.370		
	Std.	0.871	1.010	365.728		
MINCO LBFSGS	Mean	1.447	3.296	147.635	490	0.986
	Max.	9.025	5.352	697.719		
	Std.	0.909	0.647	71.668		
RRT Connect	Mean	1.687	3.560	>50000	445	0.895
	Max.	7.158	209.517	>50000		
	Std.	0.819	11.733	>50000		
STOMP	Mean	1.537	1.585	408.935	485	0.976
	Max.	30.570	4.397	5281.180		
	Std.	3.651	0.692	543.638		

VII. APPLICATIONS OF KCFRC

We applied the KCFRC algorithm to the MCTS contact planning pipeline [14] based on EISpider 4 Air hexapod robot. As illustrated in Fig. 16(a), the EISpider 4 Air features six legs, providing a total of 18 degrees of freedom (DOF). The robot has a body length of approximately 0.9m, a standing width of about 0.8m, a body standing height of about 0.24m, and a total assembly weight of 30kg. For this work, we utilized OptiTrack to acquire robot odometry and an RS Bpearl LiDAR for elevation mapping.

A. KCFRC in Legged Robot Planning

KCFRC can be used for foothold filtration during contact planning (Fig. 1). In MCTS contact state planning algorithm, candidate robot states are spawned with respect to robot reachability constraints. KCFRC can be applied to filter out unreachable footholds, eliminating contact states that cause inevitable collisions.

Beyond contact planning, KCFRC's computational efficiency enables integration with contemporary control frameworks. For **MPC integration**, KCFRC can serve as a reference generator, producing kinematically feasible swing trajectories as soft tracking constraints in whole-body optimization. For **RL integration**, KCFRC enhances learning through reward shaping, where feasible trajectories encourage collision-free swing patterns. Our method complements existing frameworks by providing preprocessing filters that reduce computational burden for subsequent planning stages.

B. Trajectory Initialization for Optimization Acceleration

In KCFRC, visibility graph is established for reachability check. Further, a poly trajectory can be initialized from it using popular search algorithms like AStar. The initialized trajectory helps a lot in accelerating the optimization process and alleviate the local minima dilemma.

To demonstrate the capability of KCFRC, we benchmark **MINCO-LBFSGS with KCFRC (proposed)** against **MINCO-LBFSGS** [34], **RRT-Connect** [32], and **STOMP** [33] planners

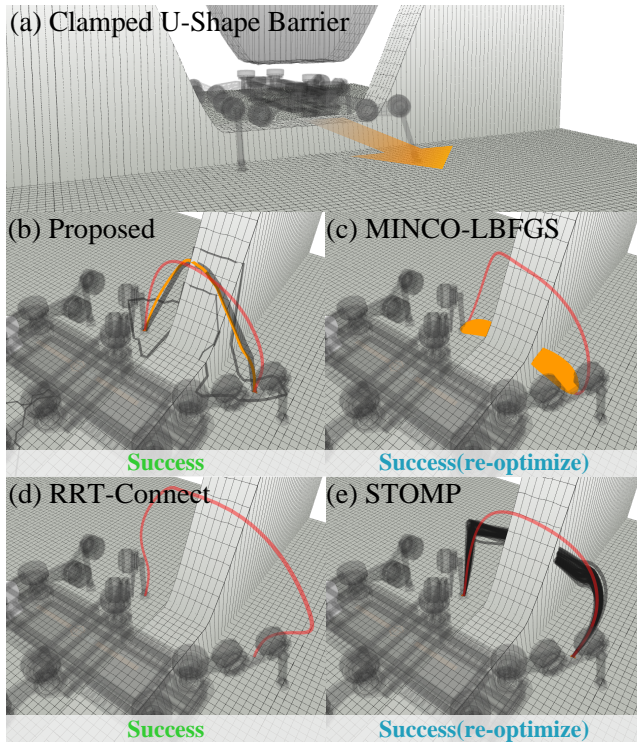


Figure 15: Comparing our proposed method with other methods in a U-shape clamped barrier planning scene considering both knee and foot collision, the final result trajectory is drawn in red. (b) The proposed planner returns a smooth swing trajectory in one shot. (c) MINCO-LBFGS optimizer returns success after many retries. (d) RRT-Connect finds a feasible swing trajectory with low quality even after interpolation. (e) STOMP returns success after many retries.

in the scenarios mentioned in the previous section. We record consumption time, trajectory length and its cost (Acc. square integration in 1s normalized time). Results are listed in Table. IV.

As the statistics show, our method is faster and steadier than any other method, and the planned trajectories take lower costs on average. However, the average length is not the shortest, because it is relevant to lift-off speed and the obstacles. Although RRT-Connect succeeds in all test cases, some of the trajectories are illegal because the time frames may not be monotone increasing, thus we count it as a failure. This is a fatal problem when deploying RRT-based planners to a space-time optimization problem.

C. Swing Trajectory Planning in Confined Space

We test swing trajectory planners mentioned above in a U-shaped clamped barrier planning scene (Fig. 15(a)). Both knee and foot collisions are considered, and the planning problem is constructed in configuration space. For the specific planning problem shown in Fig. 15, the proposed method converges rapidly from the initialized trajectory (Fig. 15(b)), while other gradient-based optimizers like MINCO-LBFGS and STOMP stuck in local minima for many times (Fig. 15(b-c)). Though

RRT-Connect finds a feasible trajectory, it is not optimal. Apparently, our proposed method generates appropriate initial trajectories so that the local-minima problem can be avoided, and it takes a shorter time to optimize.

D. Real-world Experiments

To demonstrate the capability of the KCFRC and MCTS contact planning pipeline, we conducted multiple real-world experiments on various terrains.

1) *Barrier Climbing*: As shown in Fig. 16(a), we tested the robot climbing across a barrier that is 0.12m in width and 0.19m in height, about 50% of the leg length. The orange swing trajectory is initialized from KCFRC, and the red one is the optimization result. Fig. 16(b) contains snapshots of both Rviz visualization and the real robot through the whole process. Foot SDF curves are drawn in Fig. 16(c). The SDF value means the shortest distance between the foot and the obstacles. The shortest distance of each foot during swing phases is no less than 0.02m, indicating no collisions.

2) *Stairs and Timber Piles*: The pipeline is also capable of conquering rough terrains like stairs and timber piles. Fig. 17(c1, c2) shows snapshots of the hexapod climbing up and down stairs. Each step is 0.12m high and 0.35m deep. For the timber piles in Fig. 17(a1, a2), each timber is 0.2m in width and length, with height ranging from 0.1m to 0.4m. Due to the difficulty of capturing the terrain morphology only using one Lidar, we constructed the grid map in advance. KCFRC plays an important role in avoiding leg collisions in rough terrains by offering a visibility map to initialize the swing trajectory.

3) *Hole Navigation*: The hexapod successfully climbed through a hole as shown in Fig. 17(b1, b2), demonstrating the algorithm's ability to navigate confined spaces with complex geometric constraints.

VIII. CONCLUSION

This paper addresses the Foothold Reachability Problem for legged robot locomotion in confined environments. We establish a sufficient condition for foothold reachability and implement the Kinematic Collision-Aware Foothold Reachability Check (KCFRC) algorithm, achieving notable computational efficiency. Integration with MCTS planning on the ElSpider Air 4 hexapod demonstrates effective navigation over rough terrains, while trajectory optimization acceleration is achieved through visibility graph initialization.

The proposed method has limitations, particularly regarding grid map resolution accuracy. Since intersection borders are computed on discrete grids, reachability results may miss some feasible points near borders that fall slightly outside grid boundaries. Future improvements include incorporating time dimensions into reachability checks, refining intersection border search for complex connectivity, and deploying the approach on more dynamic controllers.

REFERENCES

- [1] R. Buchanan, T. Bandyopadhyay, M. Bjelonic, L. Wellhausen, M. Hutter, and N. Kottege, "Walking Posture Adaptation for Legged Robot Navigation in Confined Spaces," *IEEE Robotics and Automation Letters*, vol. 4, DOI 10.1109/LRA.2019.2899664, no. 2, pp. 2148–2155, Apr. 2019.

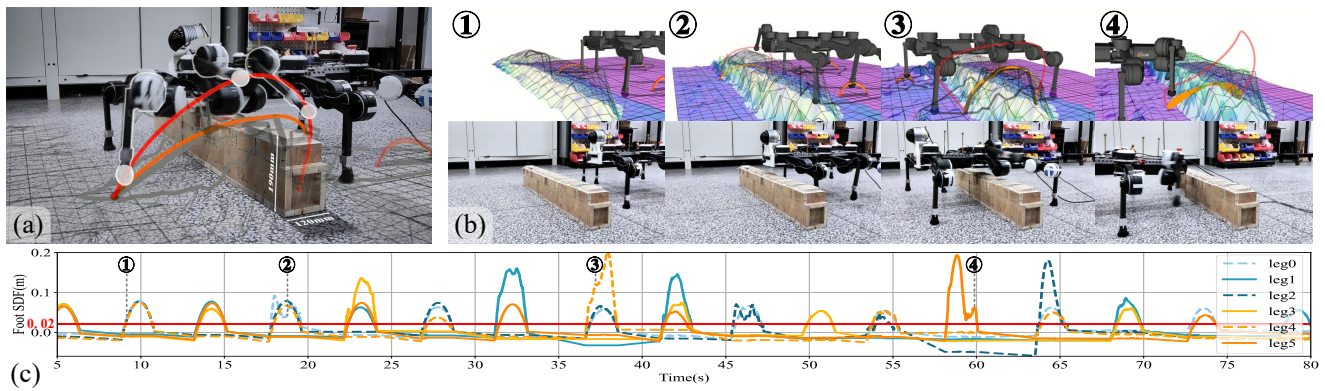


Figure 16: EISpider 4 Air climbs across a barrier. (a) The robot is getting across a barrier 0.12m in width and 0.19m in height. (b) Snapshots of the robot and Rviz visualization. (c) Foot SDF curves with time of the snapshots annotated. The SDF value of each foot during the swing phase is no less than 0.02m, claiming no unexpected collision.

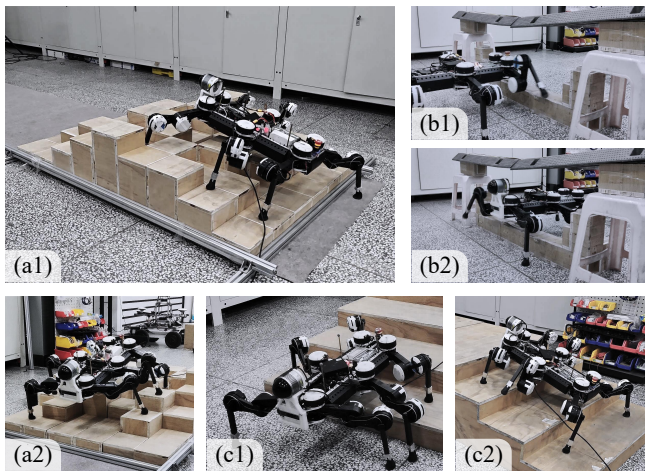


Figure 17: Real-world experimental hardware setups demonstrating KCFRC-equipped hexapod locomotion across diverse terrains. (a1, a2) Timber piles: EISpider 4 Air navigating across irregular timber obstacles with varying heights from 0.1m to 0.4m. (b1, b2) Hole navigation: Hexapod climbing through confined spaces requiring precise foothold planning and collision avoidance. (c1, c2) Stairs: Robot ascending and descending stair structures with 0.12m step height and 0.35m depth, showcasing multi-level terrain traversal capabilities.

- [2] T. Marcucci, M. Petersen, D. von Wrangel, and R. Tedrake, "Motion planning around obstacles with convex optimization," *Science Robotics*, vol. 8, DOI 10.1126/scirobotics.adf7843, no. 84, p. eadf7843, Nov. 2023.
- [3] M. Petersen and R. Tedrake, "Growing Convex Collision-Free Regions in Configuration Space using Nonlinear Programming," Mar. 2023.
- [4] B. Sundaralingam, S. K. S. Hari, A. Fishman, C. Garrett, K. V. Wyk, V. Blukis, A. Millane, H. Oleynikova, A. Handa, F. Ramos, N. Ratliff, and D. Fox, "curobo: Parallelized collision-free minimum-jerk robot motion generation," 2023.
- [5] S. Fahmi, V. Barasuol, D. Esteban, O. Villarreal, and C. Semini, "ViTAL: Vision-Based Terrain-Aware Locomotion for Legged Robots," *IEEE Transactions on Robotics*, vol. 39, DOI 10.1109/TRO.2022.3222958, no. 2, pp. 885–904, Apr. 2023.
- [6] P. Fankhauser, M. Bjelonic, C. Dario Bellicoso, T. Miki, and M. Hutter, "Robust Rough-Terrain Locomotion with a Quadrupedal Robot," in *2018 IEEE International Conference on Robotics and Automation (ICRA)*, DOI 10.1109/ICRA.2018.8460731, pp. 5761–5768. Brisbane, QLD: IEEE, May. 2018.
- [7] R. Grandia, F. Jenelten, S. Yang, F. Farshidian, and M. Hutter, "Perceptive Locomotion through Nonlinear Model Predictive Control," Aug. 2022.
- [8] T. Miki, J. Lee, L. Wellhausen, and M. Hutter, "Learning to walk in confined spaces using 3D representation," Feb. 2024.
- [9] P. Papadakis, "Terrain traversability analysis methods for unmanned ground vehicles: A survey," *Engineering Applications of Artificial Intelligence*, vol. 26, DOI 10.1016/j.engappai.2013.01.006, no. 4, pp. 1373–1385, Apr. 2013.
- [10] P. Borges, T. Peynot, S. Liang, B. Arain, M. Wildie, M. Minareci, S. Lichman, G. Samvedi, I. Sa, N. Hudson, M. Milford, P. Moghadam, and P. Corke, "A Survey on Terrain Traversability Analysis for Autonomous Ground Vehicles: Methods, Sensors, and Challenges," *Field Robotics*, vol. 2, DOI 10.55417/fr.2022049, no. 1, pp. 1567–1627, Mar. 2022.
- [11] F. Zacharias, C. Borst, and G. Hirzinger, "Capturing robot workspace structure: Representing robot capabilities," in *2007 IEEE/RSJ International Conference on Intelligent Robots and Systems*, DOI 10.1109/IROS.2007.4399105, pp. 3229–3236, Oct. 2007.
- [12] I. Akinola, J. Xu, S. Song, and P. K. Allen, "Dynamic Grasping with Reachability and Motion Awareness," Mar. 2021.
- [13] R. Buchanan, L. Wellhausen, M. Bjelonic, T. Bandyopadhyay, N. Kottege, and M. Hutter, "Perceptive whole-body planning for multilegged robots in confined spaces," *Journal of Field Robotics*, vol. 38, DOI 10.1002/rob.21974, no. 1, pp. 68–84, 2021.
- [14] P. Xu, L. Ding, Z. Wang, H. Gao, R. Zhou, Z. Gong, and G. Liu, "Contact Sequence Planning for Hexapod Robots in Sparse Foothold Environment Based on Monte-Carlo Tree," *IEEE Robotics and Automation Letters*, vol. 7, DOI 10.1109/LRA.2021.3133610, no. 2, pp. 826–833, Apr. 2022.
- [15] S. Tonneau, A. Del Prete, J. Pettre, C. Park, D. Manocha, and N. Mansard, "An Efficient Acyclic Contact Planner for Multi-legged Robots," *IEEE Transactions on Robotics*, vol. 34, DOI 10.1109/TRO.2018.2819658, no. 3, pp. 586–601, Jun. 2018.
- [16] J. Z. Kolter, M. P. Rodgers, and A. Y. Ng, "A control architecture for quadruped locomotion over rough terrain," in *2008 IEEE International Conference on Robotics and Automation*, DOI 10.1109/ROBOT.2008.4543305, pp. 811–818. Pasadena, CA, USA: IEEE, May. 2008.
- [17] M. Kalakrishnan, J. Buchli, P. Pastor, M. Mistry, and S. Schaal, "Fast, robust quadruped locomotion over challenging terrain," in *2010 IEEE International Conference on Robotics and Automation*, DOI 10.1109/ROBOT.2010.5509805, pp. 2665–2670, May. 2010.
- [18] D. Belter and P. Skrzypczyński, "Rough terrain mapping and classification for foothold selection in a walking robot," in *2010 IEEE Safety Security and Rescue Robotics*, DOI 10.1109/SSRR.2010.5981552, pp. 1–6, Jul. 2010.
- [19] X. Li, J. Li, and Y. Guo, "Foothold selection for quadruped robot based on learning from expert," in *2017 2nd International Conference on Advanced Robotics and Mechatronics (ICARM)*, DOI 10.1109/ICARM.2017.8273164, pp. 223–228, Aug. 2017.
- [20] R. J. Griffin, G. Wiedebach, S. McCrory, S. Bertrand, I. Lee, and J. Pratt, "Footstep Planning for Autonomous Walking Over Rough Terrain," in

2019 IEEE-RAS 19th International Conference on Humanoid Robots (Humanoids), DOI 10.1109/Humanoids43949.2019.9035046, pp. 9–16, Oct. 2019.

- [21] F. Jenelten, T. Miki, A. E. Vijayan, M. Bjelonic, and M. Hutter, “Perceptive Locomotion in Rough Terrain – Online Foothold Optimization,” *IEEE Robotics and Automation Letters*, vol. 5, DOI 10.1109/LRA.2020.3007427, no. 4, pp. 5370–5376, Oct. 2020.
- [22] O. Villarreal, V. Barasuol, M. Camurri, L. Franceschi, M. Focchi, M. Pontil, D. G. Caldwell, and C. Semini, “Fast and Continuous Foothold Adaptation for Dynamic Locomotion through CNNs,” Feb. 2019.
- [23] M. Zucker, N. Ratliff, M. Stolle, J. Chestnutt, J. A. Bagnell, C. G. Atkeson, and J. Kuffner, “Optimization and learning for rough terrain legged locomotion,” *The International Journal of Robotics Research*, vol. 30, DOI 10.1177/0278364910392608, no. 2, pp. 175–191, Feb. 2011.
- [24] L. Kavraki, P. Svestka, J.-C. Latombe, and M. Overmars, “Probabilistic roadmaps for path planning in high-dimensional configuration spaces,” *IEEE Transactions on Robotics and Automation*, vol. 12, DOI 10.1109/70.508439, no. 4, pp. 566–580, Aug./1996.
- [25] S. LaValle, “Rapidly-exploring random trees : A new tool for path planning,” *The annual research report*, 1998.
- [26] M. Zucker, N. Ratliff, A. D. Dragan, M. Pivtoraiko, M. Klingensmith, C. M. Dellin, J. A. Bagnell, and S. S. Srinivasa, “CHOMP: Covariant Hamiltonian optimization for motion planning,” *International Journal of Robotics Research*, vol. 32, DOI 10.1177/0278364913488805, no. 9–10, pp. 1164–1193, Aug. 2013.
- [27] J. Schulman, Y. Duan, J. Ho, A. Lee, I. Awwal, H. Bradlow, J. Pan, S. Patil, K. Goldberg, and P. Abbeel, “Motion planning with sequential convex optimization and convex collision checking,” *The International Journal of Robotics Research*, vol. 33, DOI 10.1177/0278364914528132, no. 9, pp. 1251–1270, Aug. 2014.
- [28] P. Fankhauser and M. Hutter, “A Universal Grid Map Library: Implementation and Use Case for Rough Terrain Navigation,” in *In: Robot Operating System (ROS)*, vol. 625, Jan. 2016.
- [29] J. Carpentier, G. Saurel, G. Buondonno, J. Mirabel, F. Lamiroux, O. Stasse, and N. Mansard, “The Pinocchio C++ library – A fast and flexible implementation of rigid body dynamics algorithms and their analytical derivatives,” in *IEEE International Symposium on System Integrations (SII)*, DOI 10.1109/SII.2019.8700380, 2019.
- [30] R. Diankov, “Automated Construction of Robotic Manipulation Programs,” Ph.D. dissertation, CMU, Aug. 2010.
- [31] C. B. Barber, D. P. Dobkin, and H. Huhdanpaa, “The quickhull algorithm for convex hulls,” *ACM Trans. Math. Softw.*, vol. 22, DOI 10.1145/235815.235821, no. 4, pp. 469–483, Dec. 1996.
- [32] J. Kuffner and S. LaValle, “RRT-connect: An efficient approach to single-query path planning,” in *Proceedings 2000 ICRA. Millennium Conference. IEEE International Conference on Robotics and Automation. Symposia Proceedings (Cat. No.00CH37065)*, vol. 2, DOI 10.1109/ROBOT.2000.844730, pp. 995–1001 vol.2, Apr. 2000.
- [33] M. Kalakrishnan, S. Chitta, E. Theodorou, P. Pastor, and S. Schaal, “STOMP: Stochastic trajectory optimization for motion planning,” in *2011 IEEE International Conference on Robotics and Automation*, DOI 10.1109/ICRA.2011.5980280, pp. 4569–4574, May. 2011.
- [34] Z. Wang, X. Zhou, C. Xu, and F. Gao, “Geometrically Constrained Trajectory Optimization for Multicopters,” *IEEE Transactions on Robotics*, vol. 38, DOI 10.1109/TRO.2022.3160022, no. 5, pp. 3259–3278, Oct. 2022.



Lei Ye received his Bachelor degree in Automation from Harbin Institute of Technology, Harbin, China, in 2024. He is a Master student in the Department of Aerospace Science and Technology at Harbin Institute of Technology. His research interests include legged robot planning, colony planning, and motion control.



Haibo Gao was born in 1970. He received the Ph.D. degree in mechanical design and theory from the Harbin Institute of Technology, Harbin, China, in 2004. He is currently a Professor with the State Key Laboratory of Robotics and System, Harbin Institute of Technology. His current research interests include specialized and aerospace robotics and mechanism.



Huaiguang Yang was born in 1991. He received the Ph.D. degree in the manufacturing engineering of aerospace vehicle from the Harbin Institute of Technology, Harbin, China, in 2020. He is currently an associate Professor with the State Key Laboratory of Robotics and System, Harbin Institute of Technology. His current research interests include terramechanics and dynamic simulation for planetary rovers.



Peng Xu received the Master degree in mechanical engineering from the Harbin Institute of Technology, Harbin, China, in 2020. He is currently a Ph.D. student at the State Key Laboratory of Robotics and Systems, Harbin Institute of Technology. His current research interests include motion planning, unsupervised perception, and optimal control of legged robots.



Haoyu Wang received the Bachelor’s degree in Automation from Harbin Institute of Technology, Harbin, China, in 2023. He is currently pursuing a Master’s degree in Mechanical Engineering at Harbin Institute of Technology, Harbin, China. His current research interests include optimal control of legged robots.



Tie Liu received the master’s degree in mechanical engineering in 2023 from the Harbin Institute of Technology, Harbin, China, where he is currently working toward the Ph.D. degree in the manufacturing engineering of aerospace vehicle with the State Key Laboratory of Robotics and Systems. His research focuses on the design, modeling, and simulation of Hexapod robots.



Junqi Shan is currently pursuing his Master’s degree at the State Key Laboratory of Robotics and Systems (Harbin Institute of Technology). His research focuses on intelligent path planning, optimization algorithms, and multimodal learning for robotic systems. For detailed research updates and project demonstrations, please visit his academic portfolio at <https://tipriest.github.io>.



Zongquan Deng was born in 1956. He received the master’s degree from the Harbin Institute of Technology, Harbin, China, in 1984. He is currently a Professor and an Academician of the Chinese Academy of Engineering in the Harbin Institute of Technology. His current research interests include special robot systems, and aerospace mechanisms and control.



Liang Ding (Senior Member, IEEE) was born in 1980. He received the Ph.D. degree in mechanical engineering from the Harbin Institute of Technology. He is currently a Professor with the State Key Laboratory of Robotics and System, Harbin Institute of Technology. His current research interests include terramechanics, intelligent control, design and simulation of robotic systems, in particular for planetary exploration rovers and multi-legged robots.